ELOIS Spectrometer Breadboard

ESTEC Contract N°4000109900/13/NL/SFe

Executive Summary Report

ESR

Doc. nr :	VN-ESR-AMO-HS-0053
Issue :	1
Date :	28/06/2017

	NAME	DATE	SIGNATURE
Prepared by	Amos Team	28/06/2017	
Checked by	B.BORGUET	28/06/2017	
Released by	V. MOREAU	28/06/2017	

ELOIS Spectrometer Breadboard
Final Report

Doc.: VN-ESR-AMO-HS-0053
Issue: 1
Date: 28/06/2017
Page: 2

DISTRIBUTION LIST

Name	Company	Quantity
Configuration Office	AMOS	1 copy
Vincent MOREAU	AMOS	1 soft copy
Luca MARESI	ESA	1 soft copy
Atul DEEP	ESA	1 soft copy

CHANGE RECORD

ISSUE	DATE	NB OF PAGES	MODIFIED PAGES	REMARKS
1	28/06/2017	25	All	First issue

ELOIS Spectrometer Breadboard
Final Report

Doc.: VN-ESR-AMO-HS-0053
Issue: 1
Date: 28/06/2017
Page: 3

TABLE OF CONTENTS

ELOIS Spectrometer Breadboard
Final Report

Doc.: VN-ESR-AMO-HS-0053
Issue: 1
Date: 28/06/2017
Page: 4

1. REFERENCES

1.1 SCOPE

This document reports the work that was performed by Amos, Spacebel, the Centre Spatial de Liège, Deltatec, Caeleste for the study, manufacturing, characterization and tests of a Breadboard for a Compact Free Form grating spectrometer (ELOIS). This ESA activity also covers the detailed design of a dedicated Hyperspectral CMOS sensor, the realisation of an Emulator of this sensor, and the design, manufacturing and test of its Read-out Electronics. In parallel, a Python-based simulator of the instrument performance has been developed.

It constitutes the executive summary of the ESA GSTP contract N°4000109900/13/NL/SFe originally entitled "Implementation of a Linear Variable Filter-based Hyperspectral Focal plane for Earth Observation Instrument".

1.2 APPLICABLE DOCUMENTS

[AD1]   Statement of Work   TEC-MMO/2013/48
[AD2]   ESA Contract N°4000109900/13/NL/SFe   31/03/2014
[AD3]   ESA CCN N°1 to Contract N°4000109900/13/NL/SFe   21/10/2014
[AD4]   ESA CCN N°2 to Contract N°4000109900/13/NL/SFe   30/11/2015

Doc.:	VN-ESR-AMO-HS-0053
Issue:	1
Date:	28/06/2017
Page:	5

ELOIS Spectrometer Breadboard
Final Report

1.3 LIST OF ACRONYMS AND ABBREVIATIONS

The list of Acronyms and Abbreviations used in this document is given hereunder:

AD	Applicable Documents
ADC	Analog Digital Converter
AFE	Analog Front End
AMOS	Advance Mechanical and Optical Systems
BoL	Beginning of Life
BSI	Back Side Illuminated
BRDF	Bidirectional Reflection Distribution Function
CCD	Coupled-Charge Device
CDS	Correlated Double Sampling
CMM	Coordinate Measuring Machine
CMOS	Complementary Metal-Oxide Semiconductor
CSL	Centre Spatial de Liège
CWL	Central Wavelenght
DC	Direct Current
DOP	Degree of Polarization
EGSE	Electrical Ground Support Equipment
ELOIS	Enhanced Light Offner Imaging Spectrometer
EPI	Epitaxial layer
EoL	End of Life
ESA	European Space Agency
FD	Floating Diffusion
FEE	Front-End Electronics
FFG	Free-Form Grating
FoV	Field-of-View
FP	Focal Plane
FPGA	Field-Programmable Gate Array
FWC	Full Well Capacity
FWHM	Full Width Half Maximum
GSD	Ground Sampling Distance
GSTP	General Support Technology Program
HK	HouseKeeping data
HS	Hyperspectral
LDO	Low DropOut regulators
LSB	Least Significant Bit
LSF	Line Spread Function
LVDS	Low Voltage Data Signal
LVF	Linear Variable Filter
MBS	Mixed Boundary Scan
MTF	Modulation Transfer Function
OGSE	Optical Ground Support Equipment
OoB	Out-of-Band signal
PCB	Printed Circuit Board
PGA	Programmable Gain Amplifier
PLC	Payload Computer
PTV	Peak to Valley
QE	Quantum Efficiency
RMS	Root Mean Square
ROE	Read-out Electronics
RWI	Read While Integrate
S/C	Spacecraft

SFE	Surface Form Error
SNR	Signal to Noise Ratio
SRAM	Static Random Access Memory
SPDT	Single Point Diamond Turning
SRM	Spectral Response Matrix
SWIR	Short Wavelengths Infra-Red
TM/TC	Telemetry and Telecommand
TRP	Technology Research Program
VNIR	Visible and Near Infra-Red
WFE	Wavefront Error

2. FREE FORM COMPACT SPECTRO-IMAGER

This section is a reproduction of the paper published in Conference Proceedings of 4S Symposium 2016 entitle "Tests and Calibration of a Free-Form Compact Spectro-Imager", authors : Vincent Moreau, Jorg Versluys, Michael François, Matteo Taccola, Celine Michel, Pascal Blain, Yvan Stockman.

2.1 ABSTRACT

Space-borne hyperspectral radiometers provide enhanced capabilities for environment monitoring with regards to classical multispectral missions such as PROBA V or Sentinel-2.

Small Satellite is a very attractive strategy for developing national or regional hyperspectral missions. Its low cost and rapid implementation are also valuable advantages when considering satellites constellations that can ensure the high temporal resolution required for precision agriculture and natural resources management.

The recently developed free-form grating Offner technology provides a very compact and lightweight solution for the implementation of high-performance spectrometers on a small platform. The design offers an excellent image quality while maintaining very low spectral (smile) and spatial (keystone) distortions.

The presented spectrometer consists in a fully reflective system with only three mirrors. It is a good candidate for the manufacture of an athermal instrument, with the structure and mirrors in a single material for minimizing thermal stresses.

This section presents the concept and the performances of such a spectrometer assessed on a full aluminium breadboard.

In addition to the radiometric calibration, the accuracy of the spectroscopic information depends on how well the spectral response of each pixel is known. For this purpose, the imaging and spectral performances of the spectrometer were fully characterized on a dedicated and automatized optical test bench. This characterization includes the spatial and spectral Line Spread Functions, spectral response, smile, keystone and the out-of-band rejection.

2.2 INTRODUCTION

Free-Form Optics is definitely one of the recent breakthrough in optical systems. Free-Form refers to surfaces without rotational symmetry. Such surfaces can provide important advantages in terms of optical performances and system integration. The use of Free-Form mirrors or lenses could drastically reduce the number of components in optical systems. Free-Form optics revolution is the result of developments in the theories of aberrations, in optical system optimization, and computational speed. But it is not limited to optical design, it also challenges machining, figuring, measurement and characterization processes. Ultraprecision diamond machining processes namely fast tool servo, slow tool servo and diamond milling, are frequently used to produce optical Free-Form surfaces. Furthermore, technologies like ion- beam polishing (IBF) or magneto-rheological finishing (MRF) provide the ability to fabricate Free-Form with a high surface accuracy.

One of the first full cycle pathfinder imaging system is based on a TMA design by Fuerschbach and Rolland for an LWIR imager [1]. In 2014, it was completed as a prototype demonstrator for all aspects of the technology [2].

In 2013, AMOS and ESA have introduced an original modified-Offner design for imaging spectrometer with a convex grating ruled on a Free-Form surface [3].

This study is part of a series of development undertaken by the Agency to demonstrate the feasibility of miniaturized hyperspectral instruments for mini- and nano-satellites [4, 5, 6].

ELOIS Spectrometer Breadboard
Final Report

Doc.:   VN-ESR-AMO-HS-0053
Issue: 1
Date: 28/06/2017
Page: 7

The Free-form design offers increased flexibility and throughput performances in the sense that it combines imaging, condensing and dispersing functions in a system with only three power surfaces in a very compact size. In addition, the design offers the excellent keystone and smile performances required by the application.

The originality of the design is the image reduction that has a very positive impact on the Signal-to-noise ratio. Indeed it comes with an equivalent reduction of the working F-number. For a given sensor pixel size and a given front optics aperture, the number of collected photons per pixel is multiplied by the square of the reduction factor. This is easily understood by considering that the slit width can be increased by this factor without loss of spatial resolution.
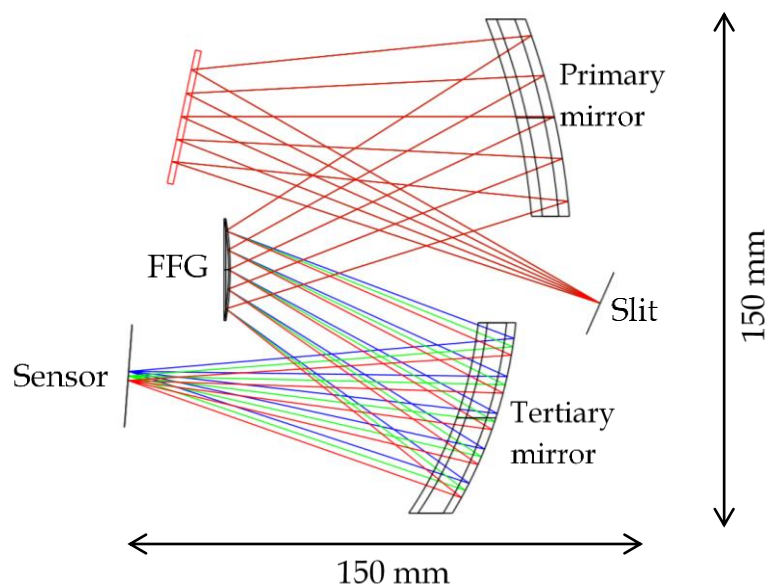
Figure 1 : Optical Design for the ELOIS Spectro-imager with Free-Form Grating

2.3 **FREE-FORM GRATING**

In 2014, we experimentally confirmed the feasibility of cost-effective manufacturing of a 35mm diameter Free-Form Grating by diamond machining on Nickel plated Aluminium substrate (Radius of Curvature : 80mm) .

By taking advantage of the most advanced ultra-precision lathe, combined with a robust control scheme, we were able to achieve the extreme axis accuracies required to maintain low straylight and scattering for gratings up to 150 lp/mm. The method provides full flexibility in selecting the blazed angle and so the wavelength at which the maximum diffraction efficiency occurs. This blaze angle is maintained constant with respect to the surface normal over the full aperture.

ELOIS Spectrometer Breadboard
Final Report

Doc.: VN-ESR-AMO-HS-0053
Issue: 1
Date: 28/06/2017
Page: 8
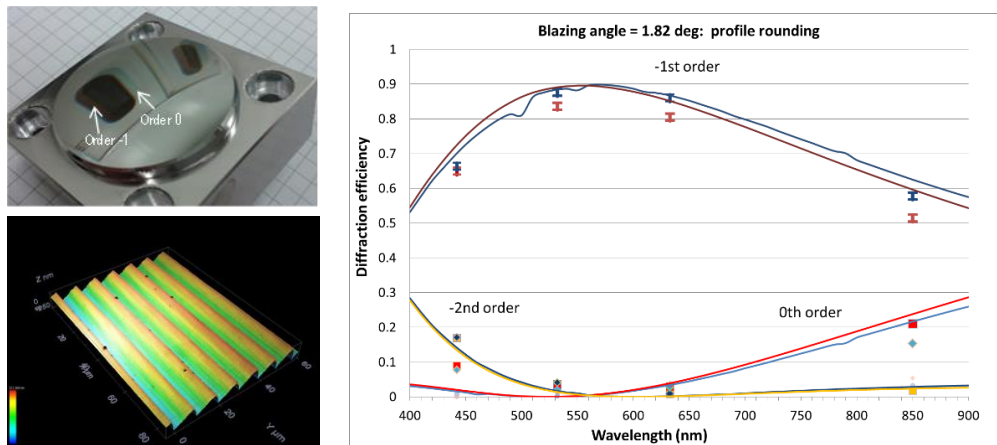
Figure 2 : Picture of the convex free form grating (top left) – Surface Profilometry by Confocal microscope (bottom left) – Measured and simulated diffraction efficiency (right)

The following performances have been measured on this Free-Form grating:

Property	Performance
Diffraction efficiency	87% max – 70% mean over VNIR
Polarization sensitivity	< 5%
Surface quality	57 nm rms SFE
Roughness	3.5 nm rms
In-plane straylight (grass)	10^{-5}

Table 1 : Measured Performances of the Free-Form Grating

2.4 SPECTROMETER BREADBOARD

Following this achievement, the Free Form grating has been tested in a complete spectro-imager instrument breadboard, with 2.5 nm spectral resolution and 15 arcsec angular resolution.

The breadboard is full aluminium, including the mirrors that were manufactured by Single Point Diamond Turning. It is composed of a lightweighted bench, with precisely rectified interfaces (±2µm planarity). The slit, the aspherical mirrors and the grating support are assembled and accurately positioned with pins and shims. An off-the-shelf CCD camera (Prosilica GE 1050), mounted on a 5 axis kinematic support completes the setup for spectral images acquisition.

The accuracy of interfaces reduces the alignment task to the absolute minimum. After assembly, the wavefront error of the system was measured, by double-pass interferometry; less than 140 nm RMS over the full field-of-view was obtained.

The entrance slit of 60 mm length and 30µm width was also produced by diamond machining, and was characterized over its full length by digital microscopy (Figure 4). The straightness is better than 1 µm and the width variation is about 1.2 µm (2-sigma values).
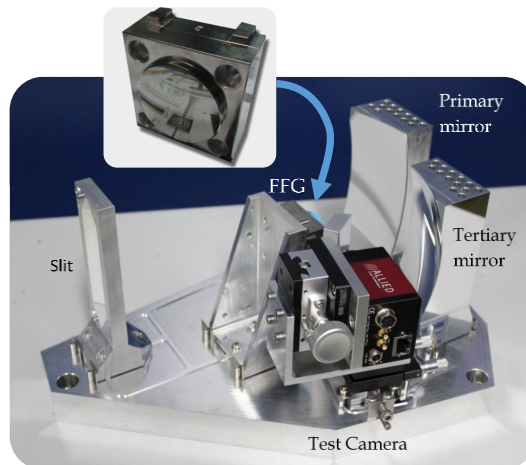
Figure 3 : Breadboard of ELOIS spectrometer, including a Free Form Grating.
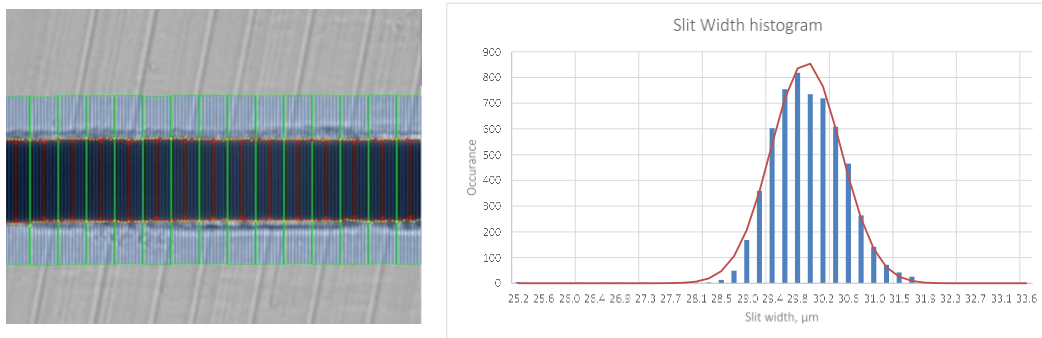
Figure 4 : Left, digital microscope image of the slit, with analyses of center and width. Right, Statistical distribution of slit width, in µm, over the full length.

2.5 PERFORMANCE AND CALIBRATION TEST SETUP

In order to characterize and validate the spectro-imager breadboard, a fully-automated optical test setup was developed with the Centre Spatial de Liege. This setup is composed of a Xenon source, a monochromator, an integrating sphere, an optical relay and various accessories (filters, polarizer, targets,…). It is able to generate either a quasi-monochromatic and uniform illumination, or the real image of a target object, at the exact location of the entrance slit. The optical characteristics of this image (angle of incidence, F/number, geometrical size, MTF) are identical to those that would be formed through a push-broom front telescope.

A dedicated software controls and synchronizes the bandwidth, the progressive scanning of incident wavelength, the camera acquisition parameters, the instrument position and the target object motion. The input irradiance is measured in real-time for the correct normalization of the acquisitions. Using this multipurpose setup with different procedures and target objects, the following performances can be measured: polarization sensitivity, line spread function (spatial resolution), spectral response function (spectral resolution), spectral registration (smile), spatial registration (keystone), out-of-band rejection (crosstalk), spectral sensitivity and straylight. In addition, the same setup can be also used for the complete characterization of the sensor camera, according to the EMVA 1288 Standard.

ELOIS Spectrometer Breadboard
Final Report

Doc.: VN-ESR-AMO-HS-0053
Issue: 1
Date: 28/06/2017
Page: 10

2.6 **TEST RESULTS**

The spectral characterization of the spectro-imager is based on the acquisition of a **3D Spectral Response Matrix S**. The elements of the Matrix S are noted $s_{i,j,\lambda}$ where i is the row index, j is the column index and λ is the monochromator wavelength index.

The S matrix is built according to the following steps:
- The bandwidth of the monochromator is set to 2.5 nm
- An acquisition S_λ, defined as the average of 16 images normalized and corrected for dark, is taken for each central wavelengths, from 435 nm to 935 nm
- Between acquisitions, the central wavelengths of the monochromator is stepped by 1 nm.

- The value of $s_{i,j,\lambda}$ is the Digital Number (DN) of the pixel (i,j) in the acquisition S_λ.

The **2D Wavelength Registration Matrix R** provides the Central Wavelength (CWL) associated to each pixel of the detector. It is calculated from the Spectral Response Matrix S, by computing for each camera pixel (i,j) the value $r_{i,j} = \lambda_{CWL} \mid s_{i,j,\lambda_{CWL}} = \max\limits_{\lambda=450 \to 900} s_{i,j,\lambda}$. In practice, sub-nanometer accuracy is achieved by Gaussian fitting of the maximum.

The spectral resolution has been computed from the R matrix to 0.167 nm/µm, giving 2.51 nm/pixel, for the 15µm square pixels of the designed instrument.

2.6.1 **Smile**

The Spectral smile Δλ is defined as the largest variation of the central wavelength along a single row (i) of the camera, i.e. $\Delta\lambda_i = \frac{1}{2}\Big(\max(r_{i,j}) - min(r_{i,j})\Big)_{j=1 \to N}$.

The instrument is specified for a smile lower than ±0.5 nm.

The value of $r_{i,j}$ along a detector row is plotted on the left of Figure 5. The fluctuation of the central wavelength from pixel to pixel is limited to less than ±0.05 nm. Over all lines, the maximum smile is about ±0.1 nm, which is well below the specification. This good figure results from the combination of excellent slit straightness and a well optimized optical design. The results also highlight the precision of the measurement, with a detection error estimated to less than 0.03 nm.
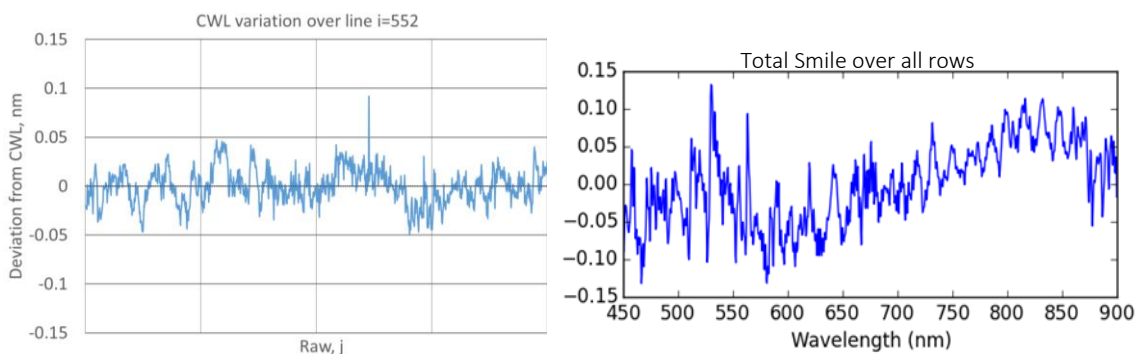
Figure 5 : Left : central wavelength deviation over a line of the sensor (mean cwl=623.7 nm) – Right : amplitude of the smile over all the lines of the sensor (referred by their mean CWL).

ELOIS Spectrometer Breadboard
Final Report

Doc.: VN-ESR-AMO-HS-0053
Issue: 1
Date: 28/06/2017
Page: 11

2.6.2 Out-of-Band rejection

The Out-of-Band rejection characterizes the cross-talk between the spectral bands for each object point within the hyperspectral image. It represents the fraction of spurious energy from radiations whose wavelengths are not within a defined bandwidth around the central wavelength of the pixel. The Out-of-Band signal is typically generated by grating scatter and ghosts.

Evaluation of the OoB signal, on each pixel (i,j) is directly obtained from matrix S :

$$OoB_{i,j} = 1 - \frac{\int_{\lambda=r_{i,j}-1.5fwhm}^{r_{i,j}+1.5fwhm} s_{i,j,\lambda}d\lambda}{\sum_{\lambda=435}^{930} s_{i,j,\lambda}} \qquad \text{Equation 1}$$

Where fwhm (Full Width Half Maximum) is the bandwidth of the specto-imager. The ELOIS spectrometer is dedicated to land and vegetation applications with a bandwidth fwhm of 10nm. The Out-of-Band rejection calculated over the detector is reported for each pixels on Figure 6. The graph on the right reports the mean value over each line (spectral coordinate). The OoB is between 3% and 5% in short wavelengths, but we can notice a rapid increase within the first lines of the sensor, corresponding to the NIR. The reason is the presence of higher order wavelengths, i.e. at a fraction of the primary wavelength. Indeed the diffraction of 800nm wavelength at order -1 occurs at the same angle than the diffraction of 400nm at order -2. In practice, an order-sorting filter (OSF) is to be added in close proximity of the sensor for removing these higher order wavelengths [7].
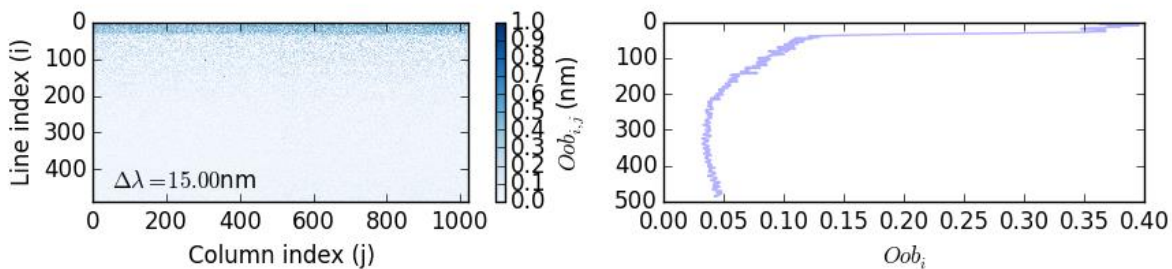
Figure 6 : Left OoB signal over the camera. Right: Mean value for each sensor line.

2.6.3 Keystone

The keystone is the measure of the deviation from straightness and parallelism of line spectra from a polychromatic point source at various positions along the slit. The keystone was measured along the whole slit length (e.g. the whole Field of View) by placing in the setup object plane a target presenting a series of 30 threads spaced by 2mm and illuminated with polychromatic light. The camera was then moved 7 times along the spatial axis in the spectro-imager focal plane in order to image the threads. Each frame exhibited the image of 6 consecutive threads while a spatial overlap of 2 threads was applied between consecutive frames to ensure the continuity of the measurements. The centroid of each threads in every frame was first roughly estimated via image segmentation. A Gaussian fit was then performed, grouping 8 consecutive detector lines together, along each column in order to precisely register the location of the maximum along the spectral direction. Each position was then fit via a 1st order polynomial. In Figure 7 we plot the variation of the slope of the fit as a function of the thread number (thread 1 and 30 corresponding respectively to the top and to the bottom of the spectro-imager slit). The maximum keystone is measured to 0.004 pixels/nm in absolute, with a test camera pixel of 5.5μm. This correspond to a keystone of ± 4.9 μm over the spectral range. The specification of keystone less than ±5μm is therefore met by the instrument breadboard.

ELOIS Spectrometer Breadboard
Final Report

Doc.: VN-ESR-AMO-HS-0053
Issue: 1
Date: 28/06/2017
Page: 12
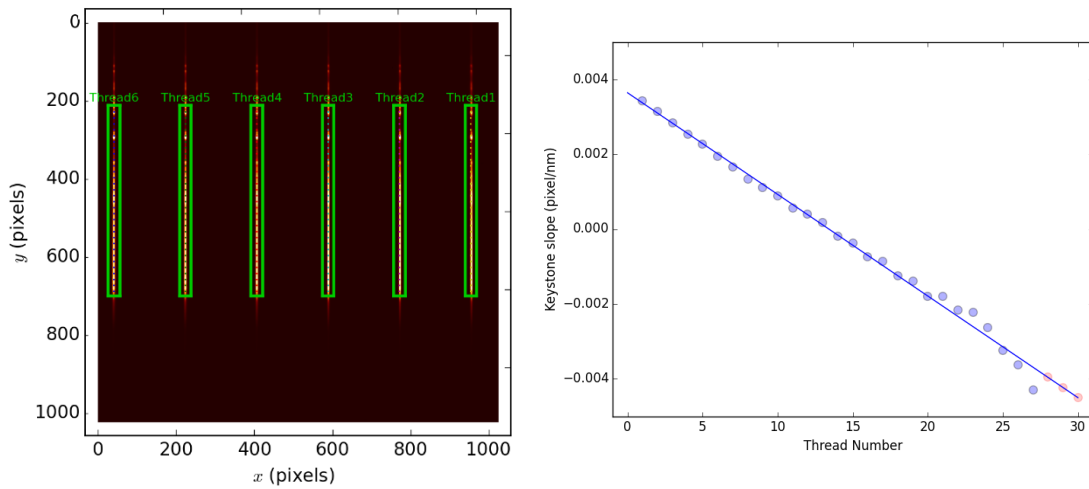
Figure 7 : Left : Determination of the local thread images positions. Right : Variation of the keystone slope across the full FOV of the ELOIS spectro-imager. The variation of the keystone slope along the slit length follows a linear law.

2.6.4 Spatial Resolution

The spatial resolution was characterized by measuring the Line Spread Function. LSF can be obtained from the scan of the entrance slit by a second orthogonal narrow slit spatially selecting the incoming light, and observing the irradiance for a fixed pixel as a function of the scan. In practice, the scanning slit has a width of 6.5 µm and a scanning step of 2 µm is chosen along 40 consecutive positions. Considering the 2:1 magnification of the instrument this translates to a scanning step of 1 µm and a slit width of 3.75 µm. In Figure 7 we present the spatial LSFs obtained for several positions along the whole slit length, from top to bottom. The measured spatial LSF is the convolution of the experimental setup profile (taking into account the finite slit width, pixel size and scanning step) by the true underlying spatial LSF of the spectro-imager. From the measured LSF, we can conclude that the setup resolution is only marginally affected by the spectrometer. The light energy is well concentrated within a 15µm diameter, confirming the good image quality measured by double pass interferometry.

ELOIS Spectrometer Breadboard
Final Report

Doc.: VN-ESR-AMO-HS-0053
Issue: 1
Date: 28/06/2017
Page: 13
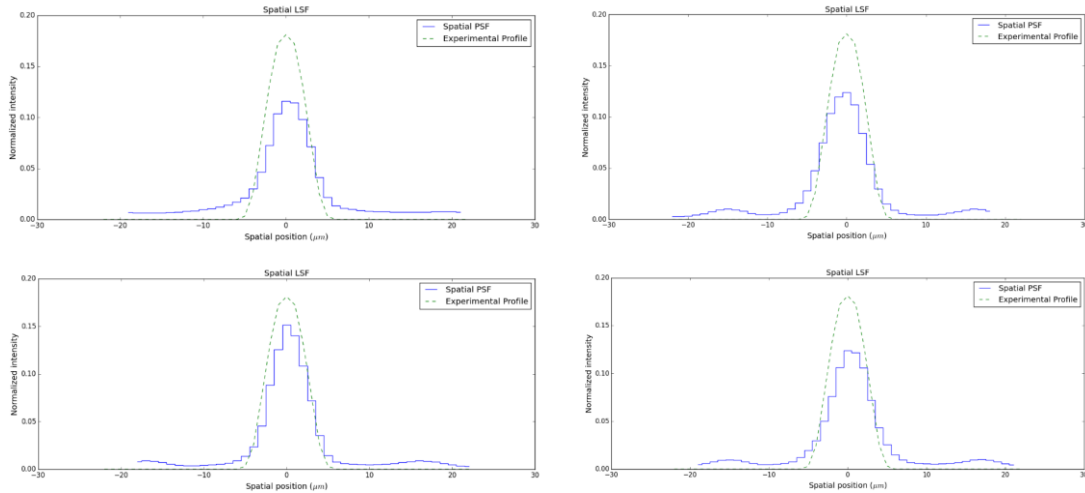
Figure 8 : Spatial LSF profile at various positions along the input slit (from top left to bottom right 4, 30, 46 and 56 mm). In dashed green we show the experimental profile (resulting from the finite detector pixel size, slit width and scanning step).

2.6.5 Spectral Resolution

The spectral LSF was obtained by illuminating the slit with a monochromatic light (0.6 nm bandwidth), scanning a narrow spectral wavelength range (typically 6 nm band) with a wavelength step of 0.2 nm. The Spectral LSF was then built by reporting the variations of irradiation of a specific pixel in the focal plane as a function of the incoming wavelength. The Spectral LSF obtained for a position along the optical axis and an incoming wavelength of 520 nm is reported in Figure 9. The FWHM of the profile is typically less than 2.5 nm, including the experimental setup contribution (convolution of monochromator bandwidth, Slit width and pixel size).
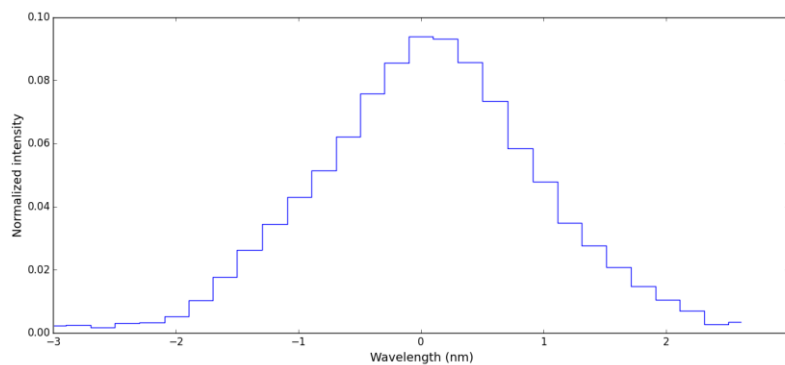
Figure 9 : Spectral LSF of the spectro-imager for a spatial location along the optical axis of the instrument and a wavelength of 520 nm.

ELOIS Spectrometer Breadboard
Final Report

Doc.: VN-ESR-AMO-HS-0053
Issue: 1
Date: 28/06/2017
Page: 14

2.7 HYPERSPECTRAL IMAGE (HYPERCUBE) ACQUISITION

We finally complete the acquisition of a Hyperspectral data cube by imaging vegetation samples placed in the object plane of the test setup. The data cube was generated by simulation of a pushbroom type scanning of the input scene by moving the whole spectro imager with increments of 30 μm (= slit width) in the along track direction. An image was captured at each scan position, as well as a single dark frame and reference illumination spectrum for the whole series of image. The result of this acquisition is reported in Figure 10. It confirms the achievement of an entirely functional device able to provide representative data that will be definitely useful for the consolidation of on-ground data process and applications assessment.

1 : Honeysuckle (Lonicera periclymenum)

2 : Bunchgrass (Brachypodium sp)

3 : Blackberry (Rubus fruticosus)
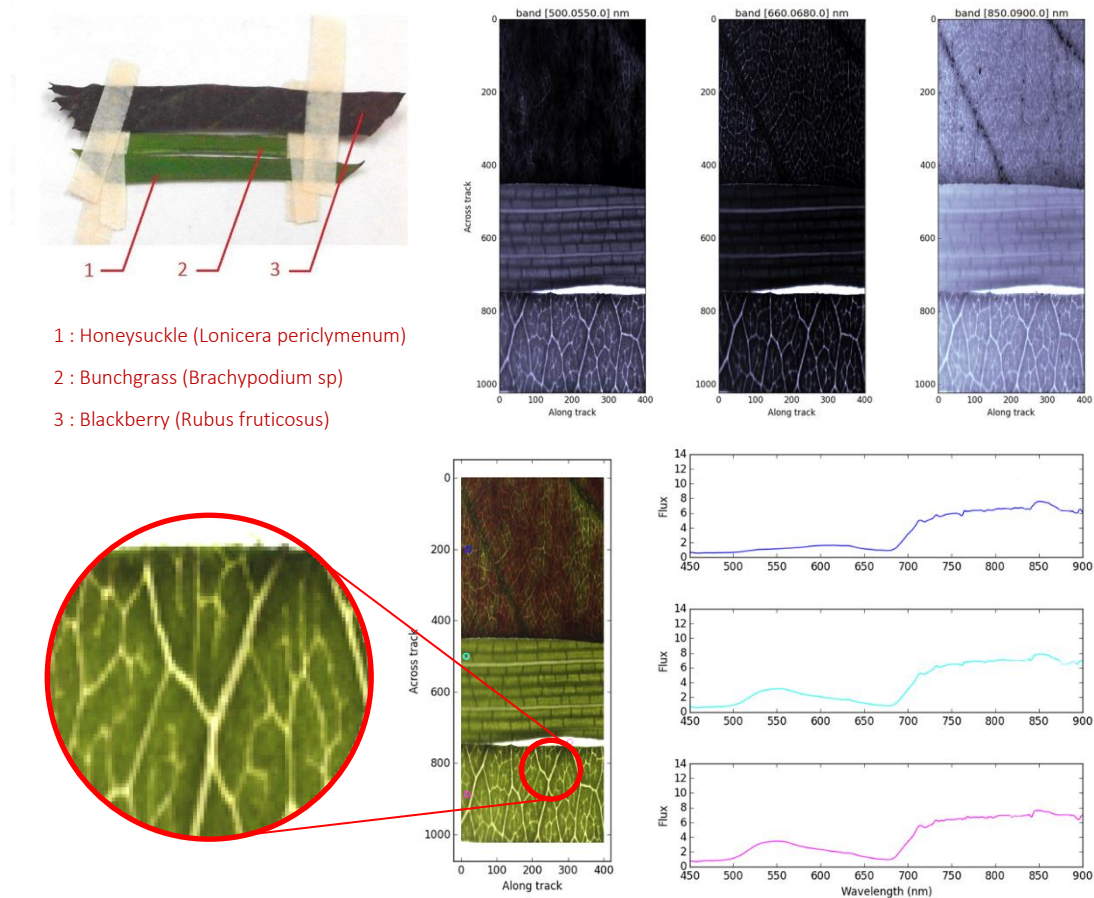
Figure 10 : Image from the HS data of 3 common leaves from understory. Top Left : Picture of the samples. Top right : Transmittance of the sample in various wavebands. Bottom left : RGB reconstructed image from the HS data with zoom on pixel level resolution features. Bottom right : spectra extracted from the HS data of the 3 leaves sample

2.8 REFERENCES

[1]. K. Fuerschbach, J. P. Rolland, K. P. Thompson, "A new family of optical systems employing φ-polynomial surfaces", Opt. Express 19 (2011), pp. 21919-21928.

[2]. K. Fuerschbach, G. E. Davis, K. P. Thompson, and J. P. Rolland, "Assembly of a freeform off-axis optical system employing three φ-polynomial Zernike mirrors," Opt. Lett. 39 (2014), pp. 2896-2899

ELOIS Spectrometer Breadboard
Final Report

Doc.: VN-ESR-AMO-HS-0053
Issue: 1
Date: 28/06/2017
Page: 15

[3]. C. De Clercq, V. Moreau, J.F. Jamoye, A. Z. Marchi and P. Gloesener, «ELOIS: an innovative spectrometer design using a free-form grating", Proc. SPIE 9626, Optical Systems Design 2015: Optical Design and Engineering VI (2015), pp. 96261O ;

[4]. L.Maresi, M.Taccola, M.Kohling, S.Lievens, "PhytoMapper Compact Hyperspectral Wide Field of View Instrument" , in book Small Satellite Mission for Earth Observation, R.Sandau ed., Springer (2010), pp 321-330

[5]. J. Blommaert, B. Delauré, S. Livens, D. Nuyts, K. Tack, A. Lambrechts, V. Morau, E. Callut, G. Habay, L. Brixhe, J. Vandenbussche, K. Minoglou, A. Deep, "CHIEM: The development of a new compact Hyperspectral Imager", to be published in Proceeding of 4S Symposium 2016.

[6]. M. Esposito and A. Z. Marchi, "HyperCube the intelligent hyperspectral imager," Metrology for Aerospace (MetroAeroSpace), 2015 IEEE, Benevento (2015), pp. 547-550.

[7]. P. Mouroulis, R.G. Sellar, D.W. Wilson, J.J. Shea and R.O. Green,"Optical design of a compact imaging spectrometer for planetary mineralogy." Optical Engineering, 46(6) (2007), pp 063001-063001-9.

ELOIS Spectrometer Breadboard
Final Report

Doc.: VN-ESR-AMO-HS-0053
Issue: 1
Date: 28/06/2017
Page: 16

3. BACKSIDE ILLUMINATED CMOS SENSOR FOR HYPERSPECTRAL IMAGING

3.1.1 Architecture and Datasheet

During the ELOIS breadboarding activity, a dedicated hyperspectral back-side illuminated CMOS sensor was designed by Caeleste. The sensor has 2022 x 256 active pixels of 15.5x15.5 µm². A high sensitivity in the visible and NIR range is important as the sensor will be used in a hyper- or multispectral imager for this range. In normal operation mode 4 adjacent rows can be binned into a lower- spectral resolution row (2.5 nm -> 10 nm). Normal shutter mode is RWI.

The following diagram shows the pixel principle:
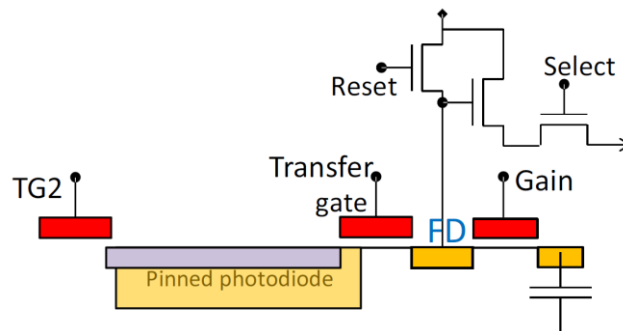
Figure 11 : Pixel Schematic

The pixel is basically a normal 4-Transistors pixel with the possibility to connect an extra capacitor to the floating diffusion or sense node. In this way a larger photodiode charge can still be in the sensor range making higher illumination levels also possible. Another addition is the second transfer gate of the pixel (TG2), not connecting to the Floating Diffusion node (FD). This addition is an anti-blooming provision and allows a greater flexibility of the sensor in terms of integration time in global shutter mode.

In binned mode, 4 pixels located vertically next to each other can be combined into a single pixel. This will be realized by shorting the FD of the 4 pixels together, and storing the combined photodiodes charges onto this common capacitance. This method is called charge domain or shared binning.

The pixel array consists of 2048 x 272 pixels of which the top and bottom 6 rows and the left and right 7 columns are blind pixels (metal covered). Electrical black pixels are also implemented and serve to compensate for row noise. Between the electrical black pixels and the normal array, 2 columns of test and variant pixels are inserted both east and west. These columns contain both electrical grey and variant pixels. The entire array will be surrounded by a two pixels wide band of guard pixels (unreadable). A minimum of 2022 x 256 pixels are normal fully sensitive pixels.

ELOIS Spectrometer Breadboard
Final Report

Doc.: VN-ESR-AMO-HS-0053
Issue: 1
Date: 28/06/2017
Page: 17
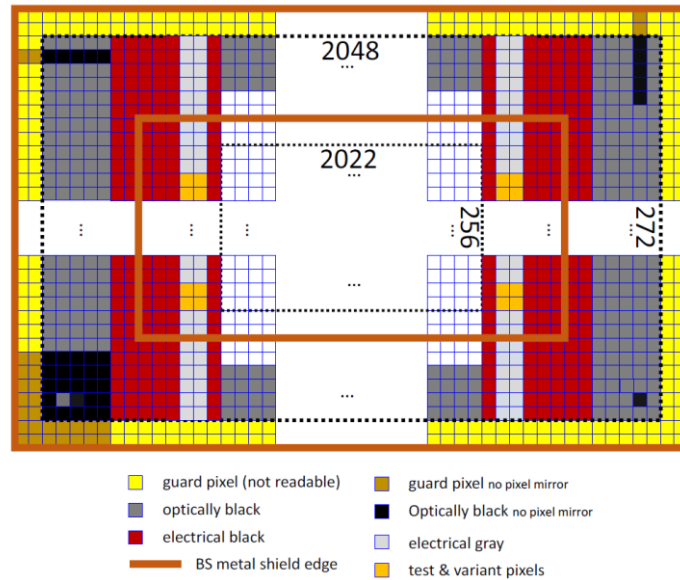
Figure 12 : Detailed pixel area

Table 2 summarizes the performances of the as-designed sensor.

Table 2 : As-design datasheet of the ELOIS sensor.

Specification	Performance
Pixel size	15.5 x 15.5 µm²
Number of Pixels	2022 x 256 pix
Shutter mode	Global
Region of Interest	Random Row access implemented
Binning	On-chip 1x4 binning
Defect pixels	< 0.01% bad ; <0.001% dead
Spectral range	400-1000 nm
Quantum efficiency	>70% @ [400nm-800nm]; >40% [800nm-900nm]
MTF	>50% at Nyquist
Read-out-noise	<160e- (full differential – with CDS)
	<180e- (pseudo differential – with CDS)
Pixel Full well capacity	250 ke- (1000ke- in binning mode)
Dark current	< 45ke-/s
Non-linearity	< 1% within 10%-90% FWC
Number of Outputs	4
Output rate	20 MHz (60 frames/s)
Power consumption	< 200 mW

ELOIS Spectrometer Breadboard
Final Report

Doc.: VN-ESR-AMO-HS-0053
Issue: 1
Date: 28/06/2017
Page: 18

In addition to the CMOS pixels, the ELOIS sensor also include extra-function detailed here below :

- Built-in test functionality: Caeleste typically integrates features allowing to test the device in-situ without needing an image. Such features include digital/analog test pattern generation on chip such as:
    - Odd/even column/line test patterns,
    - Register read-back,
    - Embedding voltages in the video stream (grey scale pixels),
    - Mixed Boundary Scan (MBS) for in-circuit signal verification,
    - MBS for readout of on-chip temperature and radiation sensors

- On-chip temperature sensors: Caeleste proposes to add 2 temperature sensors connected to MBS:
    - one with the output proportional to absolute temperature, with good Power Supply Rejection Ratio and a linear 3mV/K response. Absolute accuracy after calibration (I.e. measuring the voltage at known reference points) is about 1K.
    - one with higher sensitivity being the temperature diode in the resistor bridge, having a poorer PSRR and absolute accuracy, yet a good relative (i.e. changes over short times) accuracy that benefits from oversampling and chopping with probably better than 0.1K relative accuracy.
- Radiation degradation sensors: Caeleste will implement two radiation degradation sensors, for readout over MBS. Such are based on the "Field leakage" as being the major NMOSFET degradation mechanisms. At BOL, the output voltages are VDD, after degradation these start dropping.

3.1.2 **Quantum Efficiency and MTF**

The required high quantum efficiencies in the infra-red wavelengths are usually achieved by selecting a thick epitaxial layer. However, moving to thicker EPI layers, strongly decreases the MTF in the UV. There is an important trade-off concerning the starting material with thicker epi with better spectral response in the NIR and thinner epi favouring better MTF.

At the time of the sensor Design Review in May 2015, several options were still open to improve the QE and MTF performance of the to-be-manufactured ELOIS sensor.

Meanwhile, CAELESTE has measured BSI QE and MTF performance data from a sensor following the same production process as the ELOIS sensor.

The pixel is 4T pixel with 6.5 µm pitch and dual gain selection. The starting material is 6.5 µm EPI (ending with 4 µm EPI after BSI) normal dose and 12 µm (ending with 10.5 µm EPI after BSI) normal dose.

The graph below shows the QE curve of the sensor (plain lines are measurements; dot lines are simulations).

ELOIS Spectrometer Breadboard
Final Report

Doc.: VN-ESR-AMO-HS-0053
Issue: 1
Date: 28/06/2017
Page: 19
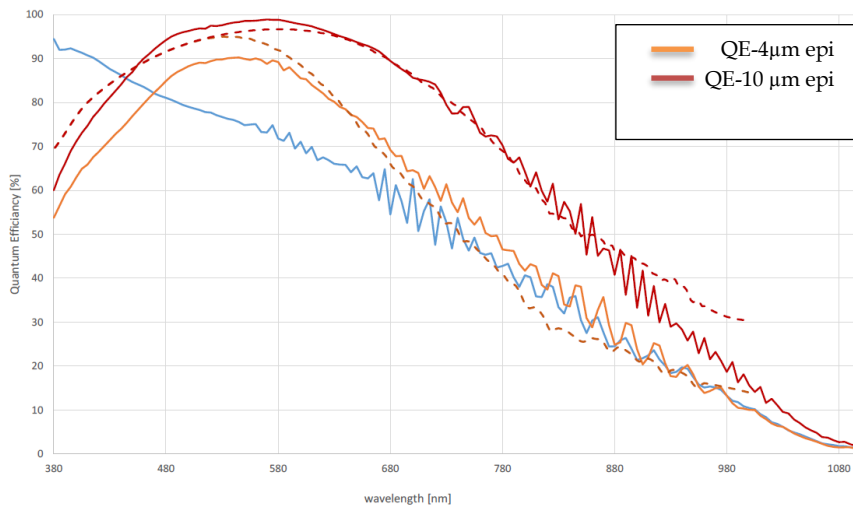
Figure 13 : BSI sensor measured curves for thin and thick epitaxial layer

The MTF for thin and thick epitaxial layer have been measured as well.

With 4 µm epi, the sensor MTF is 47 % which is close to the requirement of 50% set for the ELOIS sensor. As this MTF is reached with a 6.5 µm pixel we assume to be well in specification for a 15.5 µm pitch pixel.

For the thick EPI variant, the MTF numbers are somewhat worse than expected. Again, for the 6.5 µm pixel, the MTF is 26 % which is far from the requirement of 50% set for the ELOIS sensor. As this MTF is reached with a 6.5 µm pixel we assume the total MTF will increase for a 15.5um pixel, yet the 50% can be difficult to achieve.

The proposed solution for the next phase of the project - that will cover the manufacturing and the test of the sensor- will be to implement high resistivity thick epi, with increased depletion layer thickness and by the way a larger MTF.

ELOIS Spectrometer Breadboard
Final Report

Doc.: VN-ESR-AMO-HS-0053
Issue: 1
Date: 28/06/2017
Page: 20

4. READ-OUT ELECTRONICS

4.1 ARCHITECTURE OVERVIEW

A VNIR camera Read-out-Electronic has been designed and manufactured by DELTATEC under the ELOIS Breadboard activity. The general architecture of the camera is presented in the sketch here below:
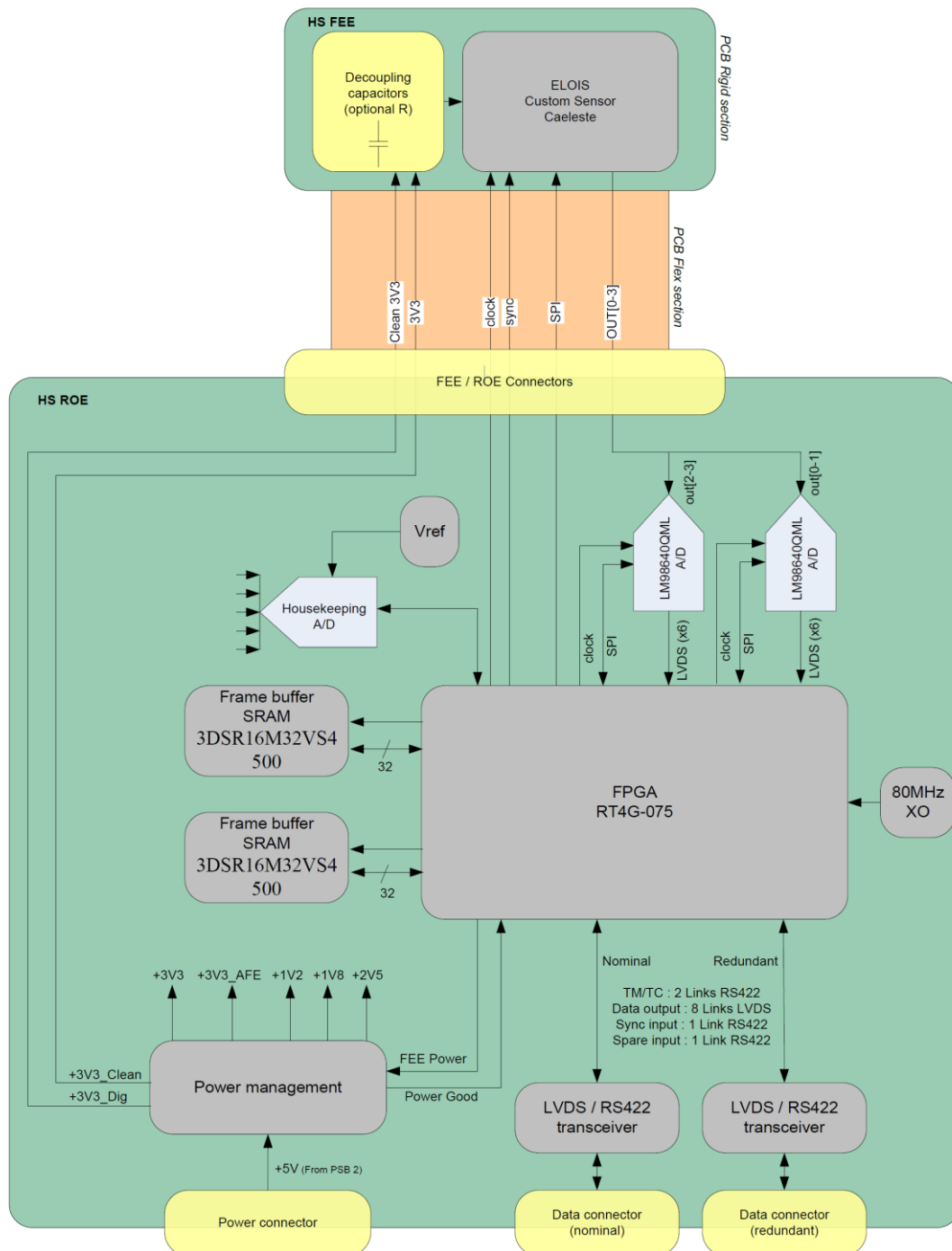
Figure 14 : Schematic of the ROE and FEE for ELOIS sensor

ELOIS Spectrometer Breadboard
Final Report

Doc.: VN-ESR-AMO-HS-0053
Issue: 1
Date: 28/06/2017
Page: 21

It is divided into two sections, the Front End Electronics (FEE) and the Read-Out Electronics (ROE).

- The FEE PCB contains only the custom ELOIS CMOS sensor and some passive components. Other active components are populated on the ROE board for thermal reasons. A micro-D connector is present for the interconnection with the ROE PCB. This PCB is a flex-rigid PCB with 2 rigid sections: main section with sensor and passive components and connector section for the FEE/ROE connector.
- The ROE contains all active components – except the detector - used for the HS channel of the instrument. A Micro-D connector is used for the interconnection with the FEE.

The selected A to D converter is the LM98640 from Texas Instrument. It supports 4 analog channels for a total frequency up to 40 Msps, with a resolution of 14bits and a SNR of 80dB. It is space qualified and interfaces with the sensor through a pseudo-differential input. Gains setting has been optimized in order to adjust with the sensor output voltage.

A frame buffer memory (SRAM) is needed to perform the Correlated Double Sampling and subsequently improve the read-out noise. The acquired reference dark pixels are stored in an external memory before being subtracted for CDS. The frame buffer is also used for the pixel reordering task.

The FPGA is the heart of the ROE. It performs different tasks:

- Sensor control
  - Pixel rate. Provides a sensor readout up to a maximum pixel rate of 80Mpixels/s (ADC clock = 20MHz). Related maximum achievable frame rate are listed in Table 3
  - Exposure time control
  - SPI configuration
  - RWI : ROE supports integrate while read operation through the use of sensor global shutter capability
  - Internal sensor binning is used as a baseline (no binning foreseen inside the FPGA).
- Correlated double sampling (CDS). The sensor is read twice. Dark frame reference is first stored in the frame buffer (external memory), then subtracted from the signal frame.
- Region of Interest readout. Spectral windowing.
- ADC control and data ingestion.
- Frame buffer management (storage of the reference dark frame).
- Data forward (after CDS) to PLC on LVDS interfaces.
- PLC TM/TC implementation.
- Image synchronization using the Line Sync input (Start of Line signal).
- ADC Housekeeping management: Variables such as sensor temperature (2x), ROE temperature, power supply voltages, Global ROE current, current limiter status and ROE mode status are to be forwarded using the PLC TM/TC link.

Initially, the foreseen flight FPGA was a rad-hard Microsemi RTAX1000-CG624-E based on the antifuse technology. But, changes in the project requirement (140Hz ->200Hz frame rate) lead to replace the FPGA to a rad-hard Microsemi RT4G-075 in CCGA1432 package which is more flexible in terms of timing (it includes an internal PLL) and resources. For the GSTP (breadboard) model, a Microsemi FPGA IGLOO 2 (M2GL090) in FG484 package is used. It has the same features but not space qualified.

The ROE is powered via a single +5V power supply line. All the needed local voltages are generated from this supply, through high efficiency DC/DCs and LDOs

A high-speed LVDS data link is used to transmit captured image data to the Payload Computer. The link must handle a data rate of 324 Mbps. Clocked at 80MHz, 5 data links are required but 6 data links are used for simplicity.

TM/TC are transmitted through RS422 driver/receiver.

ELOIS Spectrometer Breadboard
Final Report

Doc.: VN-ESR-AMO-HS-0053
Issue: 1
Date: 28/06/2017
Page: 22

The ROE Payload computer interface is required to be redundant:

- TM/TC, Sync input and LVDS data interfaces are duplicated on the ROE
- Power interface is cross-strapped in Payload computer. There is therefore only one power connector on the HS ROE.

4.2 ROE OPERATIONNAL MODE

In nominal mode, the sensor works with:

- 64 spectral bands
- 2 blind rows (not binned) -> Total of 64 + 2 rows to read
- 4 segment outputs
- Max 200 Hz frame rate
- External CDS (managed by the ROE)

For this baseline, the pixel clock will be set at 20MHz, which corresponds to a global throughput of 80 Mpixels/s.

In calibration modes, let's consider the worst case where all the rows of the detector are read (256 rows). The pixel clock remains the same.

The two modes, as tested, are summarized with their max performances in the following table:

Table 3 : Nominal and calibration mode performances (Tests results)

	Nominal mode	Calibration mode
# lines	64 + 2	256
# pixels / line	2048	2048
# pixels / segment	$512 + 9_{preamble}$	$512 + 9_{preamble}$
Pixel clock	20 MHz	20 MHz
Row time	26 µs	26 µs
Row overhead time	5.7 µs	5.7 µs
Total row time	31.75 µs	31.75 µs
CDS	External -> x2	External -> x2
Total number of lines to read	128 + 4	512
Total frame read time	4,21 ms	16,28 ms
Max achievable frame rate	237,45 Hz	61,14 Hz

It shall be noted that the maximum frame rate for the detector reading is the limiting factor for the Read-out bandwidth : SRAM and downlink have maximum frame rate higher than 250 Hz in nominal mode.

ELOIS Spectrometer Breadboard
Final Report

Doc.: VN-ESR-AMO-HS-0053
Issue: 1
Date: 28/06/2017
Page: 23

4.3 POWER BUDGET

The following table presents the ROE and FEE power budget (20 MHz pixel frequency). The power consumption is below the specification of 9 W at 200 fps.

Table 4 : Power Budget for ROE+FEE

Item	Power
ROE	6.76 W
FEE	0.13 W
TOTAL	6.89 W
Margin	20%
TOTAL with margin	8.27W

4.4 VIDEO CHAIN NOISE

The following table summarized the total Read-out noise (sensor + ROE), under the following conditions:

- 20 MHz pixel frequency
- CDS enable
- Pseudo-differential mode
- ADC working at +25°C

Table 5 : Video chain noise

	No Binning		4-pixels Binning				
	Gain 1	Gain 0	Gain 4	Gain 3	Gain 2	Gain 1	Gain 0
Full Well Capacity (ke-)	41	196	286	470	649	834	1019
Sensor Noise (e-)	11	48	59	97	133	171	208
AFE Noise (LSB)	1,79	1,79	1,79	1,79	1,79	1,79	1,79
AFE Noise (e-)	4,47	21,37	31,18	51,25	70,76	90,94	111,11
Sensor + AFE noise (x2 CDS) (e-)	13,12	56,98	73,38	120,76	166,77	214,24	260,8
Rounding noise (e-)	0.72	3,45	5,04	8,28	11,43	14,69	17,95
Total noise (e-)	13,14	57,08	73,55	121,05	167,16	214,75	261,42

These values have been considered for the system SNR analysis.

ELOIS Spectrometer Breadboard
Final Report

Doc.: VN-ESR-AMO-HS-0053
Issue: 1
Date: 28/06/2017
Page: 24

5. CONCLUSIONS AND PERSPECTIVES

Through this GSTP project, the partners have proposed an original design for a VNIR compact hyperspectral imager with excellent imaging, spectral and radiometric performances. This design benefits from using a Free Form Grating instead of a planar or spherical grating. We have confirmed experimentally the feasibility of cost-effective manufacturing of such a Free Form Grating by diamond machining on Nickel-plated aluminium substrate.

In order to validate this innovative concept, a full functional breadboard equipped with a commercial CCD camera has been manufactured and aligned. The instrument is fully athermal as all elements are made in the same material. The optics were manufactured economically with excellent quality and they were aligned easily thanks to ultra-precise interfaces and "snap-together" assembly.

An automated optical test bench has been developed for the complete characterization of the Spectro-imager. It allowed to verify the spatial and spectral performances, as well as straylight and out-of-band rejection.

In parallel, the complete design of a state-of-the-art VNIR CMOS sensor with 2048x256 pixels has been achieved. This rad-hard sensor is optimized for hyperspectral applications at 200 fps with 4 lines on-chip binning capacity, line-by-line selectable gain and very low noise.

A dedicated Read-out-Electronic for operating this sensor has been designed, manufactured and tested successfully.

By the end of this project, the VNIR Free-Form Grating Spectrometer has reached a Technology Readiness Level of 4 (Component and/or breadboard functional verification in laboratory environment)

We are convinced that this new family of compact Spectro-imager can offer valuable solutions for high performances hyperspectral missions on small satellites for earth observation and planetary exploration. The cost-effective approach is also an important advantage in the perspective of the development of future satellites constellations.

Early 2017, a new GSTP project has been started with the objective of bringing the instrument to TRL 6-8:

- to support the sensor manufacturing and Ready-to-Flight qualification (TRL8)
- to extend the design of the spectrometer up to the VNIR and SWIR wavelengths and reduce the GSD to 35 meter
- to manufacture and test a Breadboard and an Engineering Qualification Model (EQM) of the VNIR/SWIR Spectrometer Instrument.
- to perform a structural and thermal environmental campaign with the EQM and correlate the test results with the analysis (TRL6).

Specific attention will be paid to the performances that could not be fully demonstrated on the current breadboard due to the lack of representativeness, i.e. the straylight, the polarization sensitivity and the keystone.

The next figure summarized all the achievement completed by the partners during this project.

ELOIS Spectrometer Breadboard
Final Report

Doc.: VN-ESR-AMO-HS-0053
Issue: 1
Date: 28/06/2017
Page: 25

Design of a compact VNIR/PAN Instrument (AMOS)

Final design of innovative FFG Spectrometer (AMOS)

Final design HS VNIR Sensor + Emulator (Caeleste)

Final design, manufacturing and tests of ROE (Deltatec)

Full Automated Calibration and Test bench (AMOS-CSL)

Calibration software (AMOS)

Python HS instrument Simulator (AMOS)

Manufacturing and Test of ELOIS Breadboard (AMOS)

Figure 15 : Summary of the activity achievements